Applied Catalysis B: Environmental 321 (2023) 122062

Contents lists available at ScienceDirect

Applied Catalysis B: Environmental

journal homepage: www.elsevier.com/locate/apcatb

Overlooked self-catalytic mechanism in phenolic moiety-mediated Fenton-like system: Formation of Fe(III) hydroperoxide complex and co-treatment of refractory pollutants

Cheng Chen [a], Yongyi Wang [a], Yajing Huang [a], Jian Hua [b], Wei Qu [a], Dehua Xia [a,*], Chun He [a,*], Virender K. Sharma [c,*], Dong Shu [d]

[a] Guangdong Provincial Key Laboratory of Environmental Pollution Control and Remediation Technology, School of Environmental Science and Engineering, Sun Yat-sen University, Guangzhou 510275, China
[b] Guangdong Key Laboratory of Agricultural Environment Pollution Integrated Control, Guangdong Institute of Eco-Environmental and Soil Sciences, Guangzhou 510640, China
[c] Department of Occupational and Environmental Health, School of Public Health, Texas A&M University, College Station, TX 77843, USA
[d] Key Lab of Technology on Electrochemical Energy Storage and Power Generation in Guangdong Universities, School of Chemistry, South China Normal University, Guangzhou 510006, China

ARTICLE INFO

Keywords:
Self-catalysis
Fe(III)/Fe(II) redox cycling
Fe(III) hydroperoxide complex
Fenton-like reaction
Phenolic pollutants

ABSTRACT

Applications of Fenton-like reactions (Fe(III)/H_2O_2) without catalyst have low efficiency in remediating pollutants. Herein, pollutants containing phenolic moiety (P, e.g., paracetamol (PCM)) were demonstrated to make Fe(III)/H_2O_2 system highly effective in degrading a wide range of contaminants. Kinetics analysis shows the self-catalytic degradation of PCM with optimum performance at pH 4.0, and Fe(III)/Fe(II) conversion was accelerated without the assistance of cocatalyst. Based on state-of-art spectroscopy measurements and theoretical calculations, the overlooked self-catalytic mechanism was revealed. In the presence of phenolic moiety, a yellow-colored high-spin P-Fe(III)-OOH complex can be formed in Fe(III)/H_2O_2 system, which subsequently converts to Fe(II). Afterwards, the oxidation of P gives hydroquinone that also facilitates the cycling of Fe(III)/Fe(II). The accumulated Fe(II) reacts with H_2O_2 to generate hydroxyl radicals, the major species responsible to oxidize pollutants, thereby achieving efficient decontaminant performance. Results provide new insights into the self-catalytic Fenton-like process for remediating a mixture of pollutants.

1. Introduction

With the rapid development of industrialization and urbanization, a large amount of wastewater containing refractory organic pollutants is discharged into water bodies, posing a huge threat to the ecological environment and human health [1]. Phenol and its derivatives are the most widely used raw material in industrial fields such as pharmaceuticals, plastics, oil refining, coal processing and paint, and are frequently detected in effluents [2,3]. Due to their high toxicity, endocrine disrupting ability and bioaccumulation, the removal of phenolic compounds in the aquatic environment is indispensable [4,5].

Fenton and Fenton-like systems have received considerable attention in water environment remediation due to their characteristically high reaction efficiency and strong oxidation ability [6–9]. The classical Fenton system relies on the reaction between ferrous ion (Fe(II)) and hydrogen peroxide (H_2O_2) under acidic condition to generate highly reactive hydroxyl radical (•OH), the brief mechanism was expressed by Eqs. 1–5 [6,10,11]:

$$Fe(II) + H_2O_2 \rightarrow Fe(III) + OH^- + \bullet OH \; k = 40\text{–}80\ M^{-1}\cdot s^{-1} \quad (1)$$

$$Fe(III) + H_2O_2 \rightarrow Fe(II) + H^+ + HO_2^\bullet \; k = 0.001\text{–}0.020\ M^{-1}\cdot s^{-1} \quad (2)$$

$$H_2O_2 + \bullet OH \rightarrow H_2O + HO_2^\bullet \; k = (1.7\text{–}4.5) \times 10^7\ M^{-1}\cdot s^{-1} \quad (3)$$

$$Fe(III) + HO_2^\bullet \rightarrow Fe(II) + O_2 + H^+ \; k = (0.33\text{–}2.10) \times 10^6\ M^{-1}\cdot s^{-1} \quad (4)$$

$$Fe(II) + \bullet OH \rightarrow Fe(III) + OH^- \; k = (2.5\text{–}5.0) \times 10^8\ M^{-1}\cdot s^{-1} \quad (5)$$

However, Fe(II) in Fenton reagent is easily oxidized, and the conversion of Fe(III) to Fe(II) (Eq. 2) becomes the rate-limiting step [12,13].

* Corresponding authors.
E-mail addresses: xiadehua3@mail.sysu.edu.cn (D. Xia), hechun@mail.sysu.edu.cn (C. He), vsharma@tamu.edu (V.K. Sharma).

https://doi.org/10.1016/j.apcatb.2022.122062
Received 1 July 2022; Received in revised form 3 September 2022; Accepted 5 October 2022
Available online 13 October 2022

It is necessary to continuously supply Fe(II) to maintain efficient pollutant removal capacity, thus the sluggish kinetics of Fe(III) reduction and a large amount of iron sludge produced during Fenton reactions severely limit the application of Fenton processes. Compared with Fe(II)/H_2O_2 system, using Fe(III) instead of Fe(II) can reduce the operating costs and facilitate storage and transportation [14]. Similarly, accelerating the reduction of Fe(III) to Fe(II) is the key to improve the efficiency of Fe(III)-mediated Fenton-like reactions [14].

In the early years, ultraviolet (UV) or visible light irradiation was introduced to Fe(III)/H_2O_2 system. In the process of photo-assisted reaction, Fe(III) can be constantly converted into Fe(II), showing excellent performance for removing dyes [7,15–17]. To avoid energy consumption, adding organic acids, such as ascorbic acid (AA) [18], protocatechuic acid (PCA) [19], gallic acid (GA) [20,21], salicylic acid (SA) [11], and cysteine [11,22] as sacrificial reductants is another alternative option, which can complex Fe(III) and provide electrons to boost the conversion of Fe(III) to Fe(II). Nevertheless, these organic reagents are easily decomposed by ROS, at the same time, a large amount of total organic carbon in effluents may cause secondary pollution [12]. Recently, intending to facilitate the Fe(III)/Fe(II) cycle, another approach of using inorganic cocatalysts in Fenton-like system is burgeoning. Various cocatalysts such as metal sulfides/oxides (e.g., MoS_2, MoO_2, and WS_2) [23–29], zero-valent metals (Mo^0) [30] and non-metallic materials (e.g., MWCNTs [31], crystalline boron [10], and black-red phosphorus [32]) have been developed. However, the recycling and regeneration of these cocatalysts are still challenging [12].

In our paper, we present for the first time a strategy that promotes the Fe(III)/Fe(II) recycling without adding any cocatalyst, which is highly effective in decontamination. The approach was stimulated by the surprising results obtained in degrading phenolic moiety containing pollutant (paracetamol, PCM) by Fe(III)/H_2O_2 system. The phenolic constituent in PCM could propel its degradation in Fe(III)/H_2O_2 system (i.e., autocatalytic phenomena). Literature search on “self-catalysis” or “autocatalysis” determined that hydroquinone and quinone intermediates gradually generated during phenols degradation could build up a quinone cycle (Eqs. 6–9), resulting in Fe(III) reduction performance under highly acidic conditions (pH 2.0–3.0) [6,11,22,33,34]. However, the reported initiation efficiency of self-catalysis in Fe(III)/H_2O_2 system without catalyst is very low, and information on initiation mechanism is scarce. The current paper thus focused on the overlooked self-catalytic initiation mechanism and aimed at applying mechanistic understanding to reveal the high initiation efficiency of the autocatalytic degradation of phenolic pollutants in Fe(III)/H_2O_2 system under the moderate acidic condition of pH 4.0, which is at least ten times less acidic than the optimum pH condition of conventional Fenton reaction.

$$(OH)_2\text{–Ar} + \text{Fe(III)} \rightarrow \text{OH–Ar–O}\bullet + H^+ + \text{Fe(II)} \quad (6)$$

$$\text{OH–Ar–O}\bullet + \text{Fe(III)} \rightarrow \text{benzoquinone} + H^+ + \text{Fe(II)} \quad (7)$$

$$\text{benzoquinone} + HO_2^{\bullet} \rightarrow \text{OH–Ar–O}\bullet + O_2 \quad (8)$$

$$2\ \text{OH–Ar–O}\bullet \rightarrow (OH)_2\text{–Ar} + \text{benzoquinone} \quad (9)$$

The present paper is the first study on the autocatalytic phenomena of Fe(III)/H_2O_2 system induced by various emerging phenolic pollutants (P) including pharmaceutical (paracetamol), endocrine disruptor (bisphenol A) and chlorophenols (4-chlorophenol). We demonstrated the acceleration of Fe(III)/Fe(II) cycles; a vital step to carry out the Fenton reaction by continuously generating Fe(II) without a catalyst, which was overlooked in literature. Importantly, the oxidized products of P, quinones (Q) further assisted in accelerating the generation of Fe(II) from Fe(III) to continuously perform the Fenton reaction. Furthermore, a wide range of refractory pollutants could also be degraded through the phenolic moiety-mediated Fenton-like reactions. This observation of simultaneous degradation of co-existed phenolic moiety and refractory pollutants has not been reported in earlier studies. A two-step self-catalytic mechanism was proposed, based on in-depth studies including kinetics analysis, spectroscopic measurements, and identification of reactive species, as well as density function theory (DFT) calculations. The electrochemical evaluation was also applied to learn the variation of speciation of the Fe(III)/H_2O_2/P from Fe(II)/H_2O_2 system that describes higher optimum pH (i.e., 4.0) of the studied autocatalytic phenomena to degrade pollutants efficiently. This study sheds new light on the application of the phenolic moiety-mediated Fe(III)/H_2O_2 system and highlights a refreshing strategy for remediating a wide range of mixture of pollutants.

2. Materials and methods

2.1. Chemical reagents

All chemicals were of high-purity grades without further purification before use. Iron(III) nitrate nonahydrate ($Fe(NO_3)_3{\cdot}9\,H_2O$, AR, 98.5 %), paracetamol (PCM), atrazine (ATZ) and sodium hydroxide (NaOH, AR, 95 %) were purchased from Shanghai Macklin Biochemical Technology Co., Ltd. Hydrogen peroxide (H_2O_2, AR, 30 %) and nitric acid (HNO_3, AR, 65.0–68.0 %) were acquired from Guangzhou Chemical Reagent Factory. Bisphenol A (BPA), caffeine (CAF), naproxen (NPX), ibuprofen (IBP), and 4-chlorophenol (4-CP) were obtained from Aladdin Co., Ltd. China. Other chemicals and reagents are listed in Text S1 in the Supporting Information. All solutions were prepared with ultra-pure water drawn from Millipore Milli-Q water system.

2.2. Experimental procedure

The catalytic performances of Fe(III)/H_2O_2 system were evaluated via activating H_2O_2 for pollutants (e.g., PCM, BPA, 4-CP, NPX, IBP, ATZ, and CAF) removal. Typically, the pollutant degradation batch tests were conducted in a 100 mL beaker containing 50.0 mL of pollutant solution (10.0 mg/L) with magnetic stirrers (500 rpm), and the initial pH was adjusted to the presetting value using nitric acid and sodium hydroxide solutions. By successively dosing a certain amount of ferric nitrate solution (5.0 mM) and H_2O_2 (30 %), the reaction was then initiated. At fixed time intervals, 1.0 mL of the reaction solution was periodically withdrawn and filtered through a 0.22 μm polyethersulfone film. After being quenched with 0.5 mL of methanol, the samples were collected and subjected to analysis. All experiments were conducted in triplicate.

2.3. Analytical methods

The concentration of organic compounds in the samples was analyzed by high-performance liquid chromatography (HPLC, Shimadzu Essentia LC-16, Japan) with a C-18 column (WondaSil C18-WR 5 μm, 4.6 × 150 mm). The detection details such as the mobile phase and the wavelength of the UV detector were listed in Table S2. The amount of Fe(II) ion in the solution was determined by an ultraviolet-visible (UV–vis) spectrophotometer (Metash UV-5100, China) at 510 nm using 1,10-phenanthroline as the chromogenic agent (Text S2) [35]. Hydrogen peroxide concentration was measured with a modified ammonium metavanadate spectrophotometric method at 450 nm (Text S3) [36]. The oxidized products in the degradation of PCM and BPA were analyzed by an ion mobility quadrupole time-of-flight high-resolution liquid chromatography-mass spectrometer (IM-QTOF-LC-MS, Waters Synapt G2-Si, USA). More details on the above analytical methods were given in Text S4. The procedure of the density function theory calculations (DFT) is provided in Text S5. The UV–vis spectra were collected using UV–vis spectrometer (Shimadzu UV-2600, Japan). The Mössbauer spectra were collected at 12 K in transmission mode with a WSS-10 Mössbauer spectrometer (WissEl GmbH, Germany), equipped with a closed-cycle cryostat (Text S7). An electron paramagnetic resonance (EPR) instrument was applied (Bruker A300, Germany) to identify the

iron species and detect the reactive oxygen species in the system (Text S8). Open-circuit potential analysis was carried out on an electrochemical workstation (CHI 660E, China).

3. Results and discussion

3.1. Oxidation of pollutants in Fe(III)/H_2O_2/pollutants system

Initially, paracetamol (PCM), a frequently detected phenolic pharmaceutical in aquatic environment [37–39], was chosen as the model pollutant in our study, and 10 mg/L was selected as experimental concentration since this concentration is in the same order of magnitude as that of pollutants in common pharmaceutical wastewater [40]. The degradation kinetics of PCM in Fenton reaction and different Fe(III)/H_2O_2 systems fit well with the pseudo-first-order model (Fig. S1). As shown in Fig. 1a, the degradation performance at pH 4.0 is much better than that at pH 3.0 for both Fe(II)/H_2O_2/PCM and Fe(III)/H_2O_2/PCM systems. It is also worth noting that although not comparable to Fenton system, the removal efficiency of PCM in Fe(III)/H_2O_2 system almost reached 90 % within 15.0 min at pH 4.0 ($k = (1.46 \pm 0.15) \times 10^{-1}$ min^{-1}), which is better than many reported heterogeneous systems (see Table S3). Comparatively, individual H_2O_2 or Fe(III) contribute a little to the abatement of PCM (Fig. S2).

As the two main components of the system, Fe(III) and H_2O_2 are the key factors affecting the degradation performance. It can be seen from Figs. 1b and 1c that the degradation curve obtained at pH 4.0 shows a similar "S-like" shape at low Fe(III) and H_2O_2 concentrations, which is the typical feature of an intermediate-mediated self-catalytic reaction (i.e., including a lag phase of active intermediate accumulation and a subsequent rapid-increase phase) [41]. With the increase of Fe(III) dose from 10.0 to 60.0 μM, the lag phase seems to disappear gradually (Fig. 1b), and the reaction rate constant increased from $(4.57 \pm 0.34) \times 10^{-2}$ to $(1.97 \pm 0.13) \times 10^{-1}$ min^{-1}, which had a strong positive correlation with Fe(III) concentration (R^2 = 0.9966, Fig. S3). The degradation efficiency was also enhanced when higher concentration of H_2O_2 was applied (Fig. 1c). This was attributed to the fact that the high concentration of H_2O_2 is conducive to the generation of Fe(II) (see Fig. S4). Significantly, degradation of PCM at pH 2.4 and 5.0 by Fe(III)/H_2O_2 system was negligible (Fig. 1d), suggesting that the proposed self-catalytic reaction to cause the degradation of PCM was highly pH-dependent.

The variations of Fe(II) and H_2O_2 concentrations in Fe(III)/H_2O_2/PCM system are presented in Fig. 1e and f, respectively. At pH 4.0, accumulated Fe(II) from Fe(III) was ~70 % in the first 5.0 min, which then decreased with time (Fig. 1e). After 5.0 min, a decrease in the concentration of H_2O_2 was observed, indicating the reaction between Fe(II) and H_2O_2 caused the degradation of PCM (Fig. 1d). The sole Fe(III)/H_2O_2 system (i.e., without PCM) had only a small amount of Fe(II) accumulation at pH 4.0 (Fig. S5), suggesting the role of PCM in the reduction of Fe(III) to Fe(II). At pH 3.0, the accumulated Fe(II) was only ~25 %, which showed almost no decrease with time (Fig. 1e). The used concentration of H_2O_2 at pH 3.0 was also not significant (Fig. 1f), implying the minimum role of the reaction between Fe(II) and H_2O_2 at pH 3.0 to trigger the degradation of PCM. In contrast, Fe(II) accumulation and H_2O_2 decay at pH 2.4 and pH 5.0 were quite limited.

The degradation experiments with narrower pH intervals were performed (Fig. S6). The maximum value of k at pH 4.0 suggested the favorable pH to degrade PCM by autocatalytic process of Fe(III)/H_2O_2/PCM system. Moreover, the variation of solution pH during PCM degradation was monitored (Fig. S7). For the typical case of pH 4.0, the initial pH dropped to around 3.85 after the addition of Fe(III). Subsequently, with the rapid degradation of PCM, a second drop in pH occurred between 5.0 and 15.0 min. To exclude the influence of pH change on the autocatalytic reaction, the degradation experiment in acetate buffer solutions was also conducted (Fig. S8a). Due to the competitive complexation of Fe(III) by acetate [14], the degradation performance of PCM in acetate system was lower than that of non-buffer system (Figs. S6 and S8). Importantly, a similar trend in degradation efficiency was observed that the optimal pH condition was in the range of 3.6–4.0. Fig. S8b plotted k values of PCM degradation in Fe(III)/H_2O_2

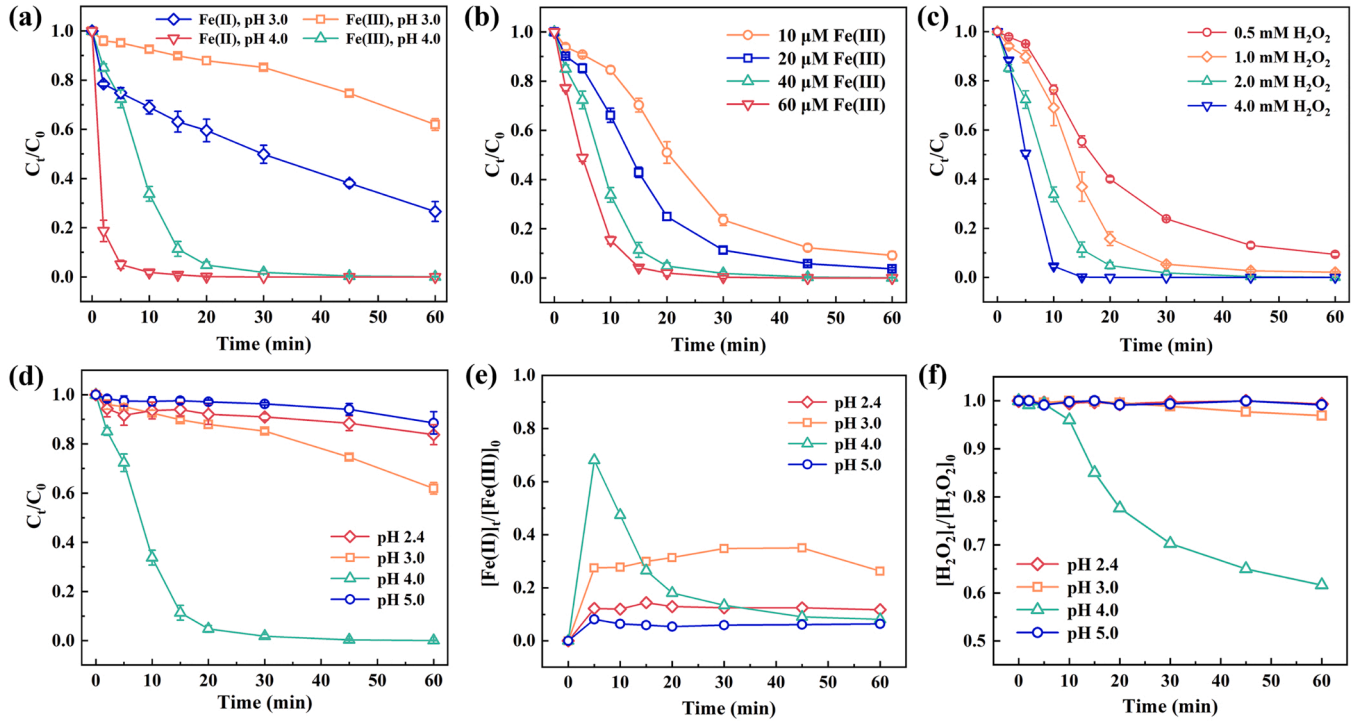

Fig. 1. Degradation of paracetamol (PCM) in (a) Fe(II)/H_2O_2 and Fe(III)/H_2O_2 systems at pH 3.0 and 4.0, and (b-d) Fe(III)/H_2O_2/PCM systems under different conditions: Fe(III) concentration (b), H_2O_2 concentration (c), pH (d), generated Fe(II) as a function of time (e), and decrease in H_2O_2 concentration with time (f) at different pH. If not otherwise specified, $[Fe(II)]_0 = [Fe(III)]_0 = 40.0$ μM, $[H_2O_2]_0 = 2.0$ mM, $[PCM]_0 = 10.0$ mg/L, pH 4.0, T = 25 °C.

system with/without buffer at different pH values, which suggested the range of moderate acidic conditions (i.e., 3.2–4.2) for effectively triggering autocatalysis.

In the next set of experiments, the autocatalytic effect in Fe(III)/H_2O_2 system was investigated by studying the oxidative degradation of other organic pollutants having different chemical structures (see Table S1). Like PCM, BPA and 4-CP contain phenolic moieties while others (NPX, IBP, ATZ, and CAF) do not have such moiety. BPA and 4-CP could be completely degraded within 45 min, similar to PCM (Fig. 2a). Comparatively, the degradation efficiency of NPX and IBP (containing benzene ring and carboxyl group) reached ~50 % in 60 min (Fig. 2a). However, no significant degradation of ATZ or CAF was observed in Fe(III)/H_2O_2 system (Fig. 2a).

The corresponding accumulation of Fe(II) and decrease in H_2O_2 containing different pollutants were monitored. In the solution containing BPA, and 4-CP, a steep peak of Fe(II) appeared within the first 20 min, indicating that Fe(III) was immediately reduced and then was able to react promptly with H_2O_2 (Fig. S9). In the case of other pollutant systems, a relatively low concentration of Fe(II) was detected (Fig. S9a) and hence hardly reacted with H_2O_2 (i.e., the consumption of H_2O_2 was not significant, Fig. S9b). The results clearly exhibited the role of phenolic moiety in autocatalytic phenomena of Fe(III)/H_2O_2 system that could able to degrade PCM, BPA, and 4-CP with high efficiency.

The participation of phenolic moiety in degrading pollutants in Fe(III)/H_2O_2 system was further explored by seeking the degradation of NPX and CAF with and without PCM (Fig. 2b and c). The degradation of NPX and CAF was dramatically enhanced in presence of PCM, while the degradation of coexisting PCM was only slightly inhibited. In addition, the removal efficiency of total organic carbon (TOC) during the co-degradation of CAF and PCM in Fe(III)/H_2O_2 system attained 80 % within 2.0 h (Fig. S10), which makes it possible to co-treat phenolic effluents and other refractory pollutants. Importantly, the degradation rates of NPX and CAF in presence of PCM were more than the degradation rate of PCM in the mixed solutions. These results suggest additional moieties besides phenolic may be existing in the mixed solution to give the enhanced autocatalytic effect of Fe(III)/H_2O_2 system that caused increased degradation of pollutants without phenolic moieties.

The additional moieties could be hydroquinone and its derivatives, which are usually formed from the oxidation of phenols by oxidants. It has been reported that hydroquinones produced during the degradation of phenolic pollutants in Fenton process can promote the reduction of Fe(III) to enhance the autocatalytic effect [16,17,33,34]. In our study, we first performed experiments to identify the formation of such hydroquinones in the degradation of PCM and BPA by the autocatalytic process. The identified structures of the oxidized products are listed in Tables S4–S5, and the mass spectra are given in Figs. S11–S12. The DFT calculations were performed as a guide to learn pathways to give different oxidized products (Text S5, Figs. S13 and S14) [42]. The possible pathways of the degradation of PCM and BPA are presented in Fig. S15 and Text S6. It could be seen that phenol and *p*-benzoquinone as well as their derivatives were detected during the degradation of PCM and BPA by Fe(III)/H_2O_2 system. It is worth mentioning that phenol and *p*-benzoquinone produced may easily trigger a quinone cycle, which could lead to the acceleration of Fe(III)/Fe(II) cycle in Fe(III)/H_2O_2 system.

The possible role of hydroquinones was learned by carrying out the

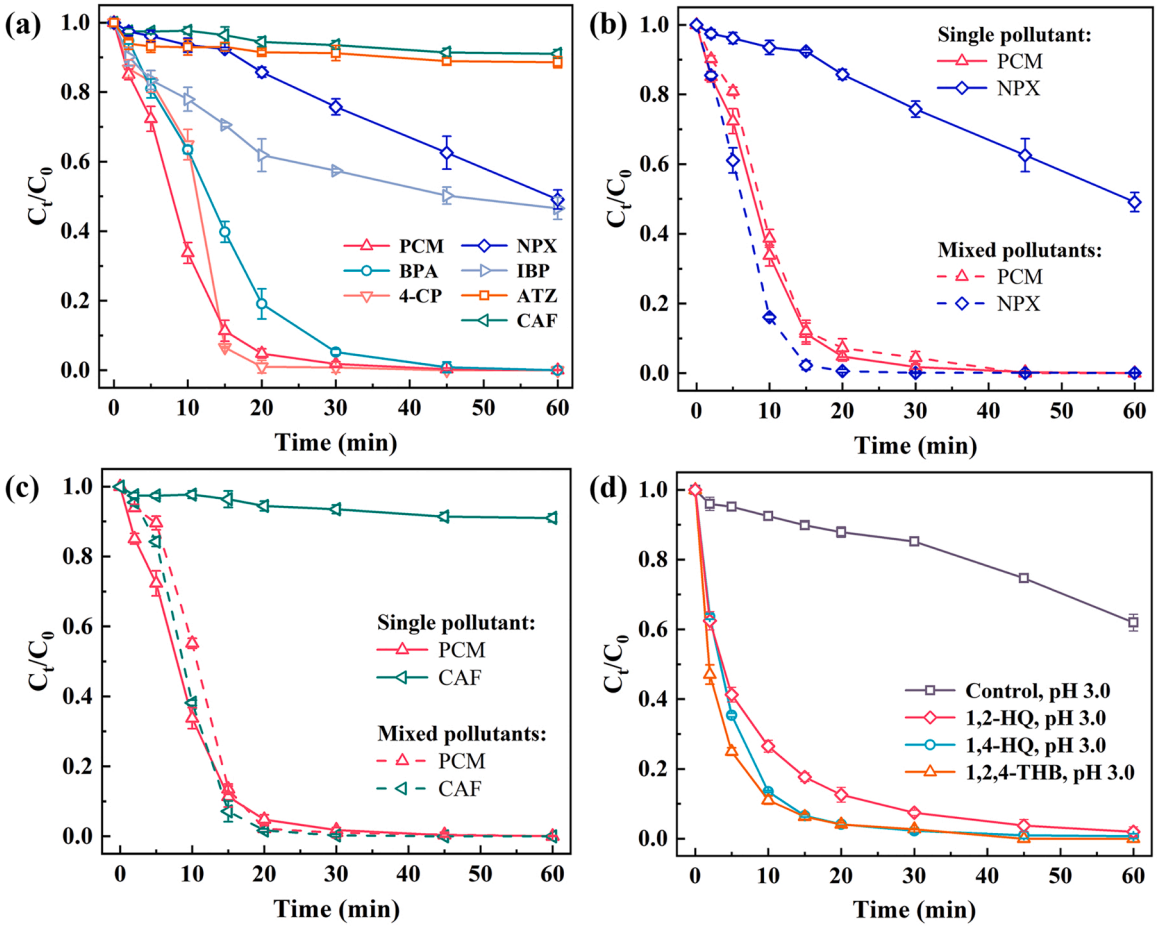

Fig. 2. Degradation of pollutants in Fe(III)/H_2O_2 system: (a) different pollutants, (b) NPX with and without PCM, (c) CAF with and without PCM, and (d) effect of added hydroquinones on PCM degradation. If no special note, initial pH 4.0, $[H_2O_2]_0$ = 2.0 mM, $[Fe(III)]_0$ = 40.0 μM, $[Pollutant]_0$ = 10.0 mg/L, $[1,2\text{-HQ}]_0$ = $[1,4\text{-HQ}]_0$ = $[1,2,4\text{-THB}]_0$ = 2.0 mg/L, T = 25 °C.

degradation of PCM in Fe(III)/H_2O_2 system with the addition of polyphenol-type compounds such as 1,2-hydroquinone (1,2-HQ), 1,4-hydroquinone (1,4-HQ) and 1,2,4-trihydroxybenzene (1,2,4-THB) (Fig. 2d). The addition of 1,2-HQ, 1,4-HQ and 1,2,4-THB remarkably improved the degradation efficiency of PCM at pH 3.0, and the corresponding reaction rate constants were determined as $(1.28 \pm 0.07) \times 10^{-1}$ min^{-1}, $(1.99 \pm 0.02) \times 10^{-1}$ min^{-1} and $(2.12 \pm 0.13) \times 10^{-1}$ min^{-1}, respectively. The increased k values could be ascribed to the rapid accumulation of a large amount of Fe(II) under the same conditions (Fig. S16). In addition, after adding these polyphenol compounds, H_2O_2 concentration in the solution quickly decreased without a lag phase (Fig. S17). The degradation of NPX in presence of 1,4-HQ was also studied. As shown in Fig. S18, the degradation of NPX by Fe(III)/H_2O_2 system is enhanced with the addition of 1,4-HQ, supporting the role of oxidized products of parent phenolic compounds.

Results show that phenolic and hydroquinone compounds were conducive to the degradation of pollutants in Fe(III)/H_2O_2 system. These compounds likely formed complexes with Fe(III) in Fe(III)/H_2O_2 system prior to generating the reactive species to oxidize pollutants at pH 4.0. This is discussed in the next section.

3.2. Formation of Fe(III) complex in the initiation of autocatalytic process

Intriguingly, when the solution of Fe(III), H_2O_2, and phenolic pollutant were mixed, we were surprised to find that the color changed. Taking PCM as an example (Fig. S19a), the solution color first changed from colorless to pale yellow within 5.0 min. Significantly, this time of the obvious yellow appearance coincides with the rapid degradation period of pollutant (Fig. 1a and Fig. S19a). With the progress of the reaction, the yellow color gradually disappeared and finally returns to original colorless after 60 min (Fig. S19a). Importantly, no yellow color was observed when NPX, IBP, ATZ, and CAF were degraded in Fe(III)/H_2O_2 system (Fig. S19b). The emergence of yellow intermediates seems to be the initiation of autocatalytic process, which were characterized using spectroscopic techniques as described below.

UV–vis spectra of the mixed solutions under different reaction conditions were collected. The change of absorbance spectra of Fe(III)/H_2O_2/PCM mixture with time at different PCM concentrations (10.0–100.0 mg/L) are shown in Fig. S20. A broad shoulder in the range from 400 to 500 nm appeared at 4.0 min, then became inconspicuous, and the absorbance gradually decreased, which was consistent with the depletion of PCM in the mixed solution (see Fig. 1). No shoulder peak was observed in the mixed solution of Fe(III) and PCM (i.e., without H_2O_2) (Fig. S21), indicating the involvement of H_2O_2 in the formation of shoulder peak of the complex. As shown in Fig. 3a, with the increase of PCM concentration, the shoulder peak with a maximum of 436 nm became more pronounced. The linear correlation between the absorbance at 436 nm and PCM concentration was found (inset Fig. 3a), which explicitly indicated that the shoulder peak is attributed to the formation of a kind of iron complex, in which PCM molecule serves as

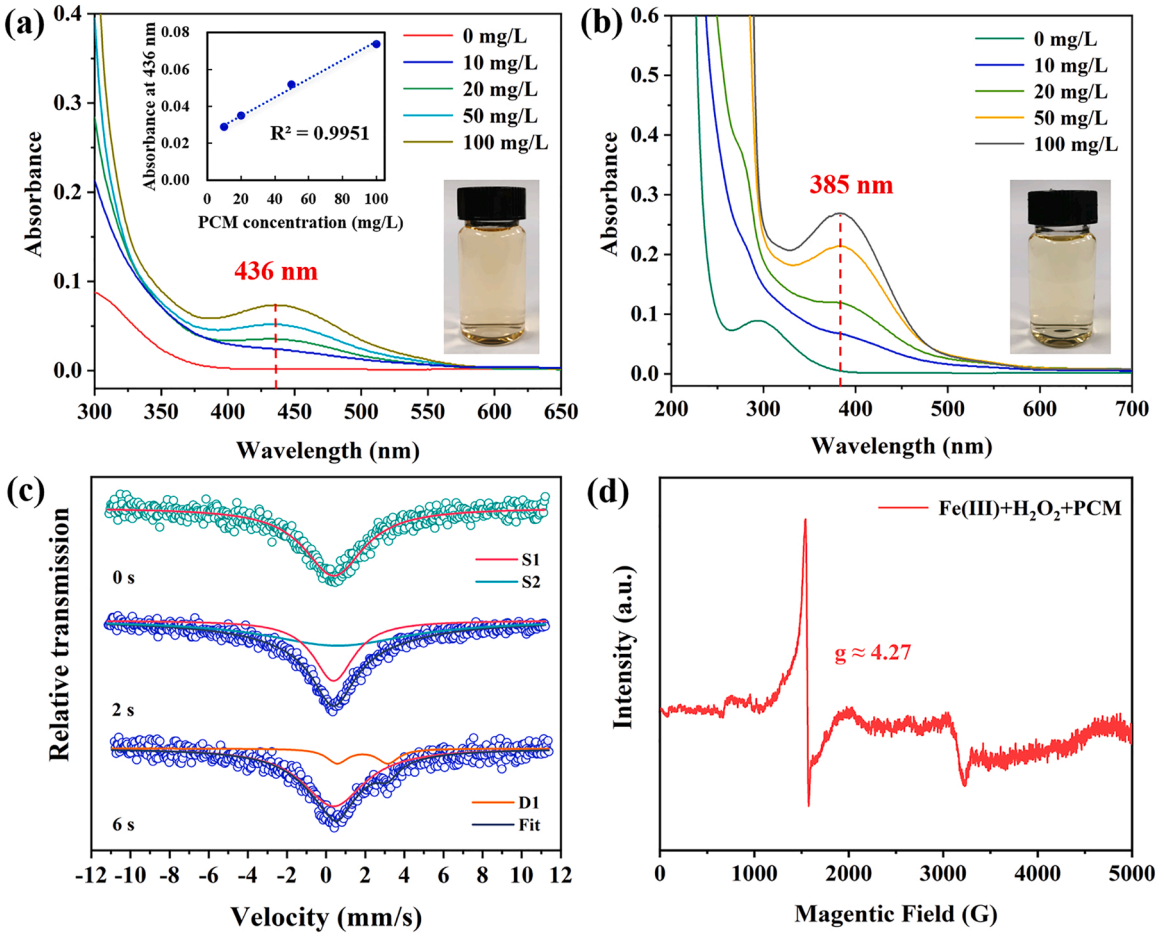

Fig. 3. (a) UV–vis spectra of Fe(III)/H_2O_2/PCM system at different PCM concentrations, inset: relationship of absorbance at 436 nm to pollutant concentration at 4.0 min and photo shows the mixed solution color of Fe(III)/H_2O_2/PCM system at 4.0 min; (b) UV–vis spectra of Fe(III)/H_2O_2/BPA system at different BPA concentrations, inset: photo shows the mixed solution color of Fe(III)/H_2O_2/BPA system at 4.0 min ($[Fe(III)]_0$ = 40.0 μM, $[H_2O_2]_0$ = 2.0 mM, pH 4.0). (c) Mössbauer spectrum of Fe(III) (green) and Fe(III)/H_2O_2/PCM mixture (blue) ($[PCM]_0$ = 15 g/L, $[Fe(III)]_0$ = 0.5 M, $[H_2O_2]_0$ = 0.8 M). (d) Low-temperature (T = 98 K) EPR spectrum of Fe(III)/H_2O_2/PCM mixture. ($[PCM]_0$ = 100.0 mg/L, $[Fe(III)]_0$ = 40.0 μM, $[H_2O_2]_0$ = 2.0 mM, pH 4.0).

the ligand and H_2O_2 may play an essential role [43,44]. The participation of PCM in the formation of this complex was further confirmed by Fig. S22 that the increase of PCM concentration led to a longer absorbance rise period at 436 nm. Interestingly, similar results were also found in Fe(III)/H_2O_2/BPA system (Fig. S23). Higher BPA concentration resulted in higher maximum absorbance and delayed the appearance of peak time. The maximum absorption wavelength of the shoulder peak varies with the nature of the pollutant, which is 385 nm in Fe(III)/-H_2O_2/BPA system (Fig. 3b). In cases of mixed solutions of Fe(III)/-H_2O_2/NPX and Fe(III)/H_2O_2/CAF, no shoulder peaks were seen (Fig. S24). As the hydroquinone compound, the pure 1,4-HQ solution exhibited a characteristic peak at 288 nm, while when Fe(III) and H_2O_2 were involved, a shoulder peak at 500 nm attributed to Fe(III) hydroperoxide appeared (Fig. S25) [43].

The oxidation state of iron of the yellow complex in Fe(III)/H_2O_2/PCM system was determined by applying iron-57 Mössbauer spectroscopy technique. The results are shown in Fig. 3c and Table S8. The spectrum of frozen Fe(III) solution displayed a singlet (S1) with an isomer shift (IS, δ) of 0.393 mm/s. After mixing Fe(III) with H_2O_2 and PCM for 2.0 s, a newly broadened singlet with an isomer shift of 0.594 mm/s appeared (S2), which was similar to those reported for monomeric high-spin Fe(III) in iron complex [45–47]. However, after a few more seconds of mixing (i.e., 6.0 s), the spectrum of the mixture showed a brand-new doublet (D1). With the larger IS value (1.868 mm/s) and quadrupole splitting (QS, Δ) of 2.590 mm/s, D1 was assigned to the high-spin Fe(II) species [48–50]. These results indicated that a ferric complex was first formed in Fe(III)/H_2O_2/PCM system, which was then promptly converted into Fe(II) species. A low-temperature EPR spectroscopy technique was also applied to learn the nature of the transient yellow complexes. As shown in Fig. 3d, a rhombic spectrum appears at approximately 1200–1900 G with a *g* factor of 4.27, which could be ascribed to the high-spin Fe(III) center in Fe(III) hydroperoxide[44,51, 52].

The spectroscopy results of the yellow complex clearly exhibited the participation of phenolic ligand and H_2O_2 in the Fe(III) complex. The yellow intermediates were proven to be high-spin ferric hydroperoxide complexes, defined as P-Fe(III)-OOH, where P represents the specific phenolic pollutant ligand. The yellowing of solution may be assigned to -O-O-→Fe(III) ligand-to-metal charge transfer (LMCT) transition in Fe (III) hydroperoxide complexes [41,44].

To further confirm the critical role of PCM-Fe(III)-OOH, several ions were introduced to interfere with the formation of PCM-iron(III) hydroperoxide. Aluminum ion (Al^{3+}) and zinc ion (Zn^{2+}) were used as cationic competitors of PCM ligand, which decreased the values of *k* by 50.5 % and 64.1 %, respectively (Fig. S26). No decrease in concentration of PCM was observed when $H_2PO_4^-$ was added (Fig. S26b), due to the strong complexation of Fe(III) and $H_2PO_4^-$ ($\log K_{Fe(III)-H_2PO_4^-} = \sim 3.5$) [52]. These results implied that the participation of the yellow PCM-iron (III) hydroperoxide is indispensable to perform the autocatalytic process. These complexes must be decomposed to give reactive species to degrade pollutants. Next, the identification of the reactive species was performed and described below.

3.3. Identification of involved reactive species

Recently, an increasing number of studies suggested the existence of high-valent iron species (Fe(IV)=O^{2+} or Fe(V)=O^{3+}) in multiple homogeneous [53–55] and heterogeneous [56–59] iron-based AOPs. Therefore, we first explored the formation of high-valent iron species in Fe(III)/H_2O_2 system. Methyl phenyl sulfoxide (PMSO) was selected as the probe agent to detect the high-valent iron species in Fe(III)/H_2O_2 system. PMSO can be oxidized by high-valent iron species to the corresponding methyl phenyl sulfone ($PMSO_2$) via oxygen transfer [60]. As depicted in Fig. S27, no conversion from PMSO to $PMSO_2$ was observed in either Fe(III)/H_2O_2 or Fe(III)/H_2O_2/PCM system. Results excluded the generation of high-valent iron species, which is consistent with previous work [10].

Next, the generation of reactive oxygen species (radicals and singlet oxygen) in the system was investigated. First, quenching tests for •OH, $HO_2^•/O_2^{•-}$ and $^1O_2$ were conducted to evaluate the contribution of each species during the oxidation of PCM in Fe(III)/H_2O_2 system. Tert-butyl alcohol (TBA), which has no α-hydrogen, is the typical scavenger for •OH ($k_{TBA+•OH} = (3.8–7.6) \times 10^8\ M^{-1}{\cdot}s^{-1}$) [25,61]. Chloroform ($CHCl_3$, $k_{CHCl_3+HO_2^•/O_2^{•-}} = 3.0 \times 10^{10}\ M^{-1}{\cdot}s^{-1}$) [62] is used as $HO_2^•/O_2^{•-}$ scavenger, while L-histidine ($k_{L-histidine+O_2} = 1.5 \times 10^8 M^{-1}s^{-1}$) [63,64] and furfuryl alcohol (FFA, $k_{FFA+^1O_2} = 1.2 \times 10^8 M^{-1}s^{-1}$) [56,65,66] are used to quench $^1O_2$. As depicted in Fig. 4a, no matter what kind of quencher (20.0 mM) was added, the reaction could be severely suppressed. This was an unexpected result; hence, we inferred that the quencher interfered with the reaction progress. This was confirmed by monitoring Fe (II) accumulation and levels of H_2O_2 in Fe(III)/H_2O_2/PCM system in presence of quenchers (Fig. S28). The addition of quenchant did affect the accumulation of Fe(II). Also, the decrease in H_2O_2 concentrations was inhibited to varying degrees in presence of different quenchants. To weaken these additional effects of quenchants on ROS recognition, quenching experiments with lower quencher concentration (i.e., 5.0 mM) were carried out. Results of Fig. S29 suggest that, except for TBA, the degradation ability of the system to oxidize PCM was restored when the dosage of quenchers was reduced to 5.0 mM. TBA could still prevent the oxidation of PCM, indicating that •OH likely played a major role in Fe(III)/H_2O_2 system.

The formation of •OH, $HO_2^•/O_2^{•-}$, and $^1O_2$ in the system were also studied by electron spin-resonance (ESR) spectroscopy method using DMPO and TEMP as trapping agents. As shown in Fig. S30, the characteristic signals of DMPO-•OH, DMPO-$HO_2^•/O_2^{•-}$, and TEMP-$^1O_2$ triplet were detected; these three species were generated in Fe(III)/H_2O_2 system. Fig. 4b displayed the ESR spectra for detecting •OH in Fe(III)/H_2O_2 system at different pH and in the presence of PCM. DMPO-•OH adduct with an intensity ratio of 1:2:2:1 was observed at both pH 3.0 and 4.0, and the signal was stronger at pH 4.0, which was consistent with the superior degradation ability of Fe(III)/H_2O_2 at pH 4.0. Moreover, once PCM was added, the characteristic signal became much weaker, indicating that •OH was greatly consumed to degrade the pollutant. In contrast, the ESR signal appeared to be unaffected by the addition of CAF to Fe(III)/H_2O_2 system (Fig. S31), which was consistent with the fact that CAF could be hardly degraded in Fe(III)/H_2O_2 system (Fig. 2a).

$HO_2^•/O_2^{•-}$ is another possibly formed ROS in Fe(III)/H_2O_2 system. Due to the relatively slow reaction kinetics ($k_{phenol+HO_2^-/O_2} = 5.8 \times 10^2 - 2.7 \times 10^3 M^{-1}{\cdot}s^1$) [67], its contribution to PCM degradation is rather finite, thus $HO_2^•/O_2^{•-}$ could not be the main ROS in Fe(III)/H_2O_2 system. Since the lifetime of $^1O_2$ can be prolonged for at least 10 times by changing the solvent from H_2O (2.9–4.6 μs) to D_2O (22–70 μs) [53,68], PCM degradation test was carried out in D_2O solvent to further distinguish the role of $^1O_2$. However, as shown in Fig. S33, no enhancement of PCM degradation performance was observed, which means that $^1O_2$ only had a subtle contribution to PCM elimination. In conclusion, •OH is the primary reactive species in Fe(III)/H_2O_2 system and plays a notably vital role in PCM degradation. The concentration of •OH was next determined.

To track the generation of •OH, the semi-quantitative analysis test was conducted using terephthalic acid (TPA) as the chemical probe, which can react with •OH via H abstraction to form 2-hydroxyterephthalic acid (HTPA) [10]. Figs. S34 and 4c illustrated the variations of TPA and HTPA in different Fe(III)/H_2O_2 systems. The concentration of TPA decreased gradually, indicating that TPA was gradually transformed or degraded during the reaction. In the meantime, the concentration of HTPA first increased to the maximum and then decreased. This trend was attributed to the conversion of TPA to HTPA in the initial stage, and the excessive •OH could also gradually degrade HTPA [69]. It should be noted that the generation rate of HTPA at pH 4.0 was

generally greater than that at pH 3.0, which was consistent with H_2O_2 being more likely activated at pH 4.0 to produce •OH. With the change of color, the introduction of PCM at pH 4.0 not only aggravated the decay of TPA, but also strikingly accelerated the accumulation and decomposition of HTPA. Whereas the existence of PCM in Fe(III)/H_2O_2 system at pH 3.0 exhibited feeble impetus to •OH generation.

Fig. 4d depicted time profiles of HTPA concentration, Fe(II) accumulation, and absorbance at 436 nm. The absorbance at 436 nm and Fe (II) concentration reached their maximum values at 4.0 min and 5.0 min, respectively. The maximum HTPA concentration appeared after 10 min. These results indicate that the production of PCM-Fe(III)-OOH precedes the reduction of Fe(III), which also means the formation of PCM-Fe(III)-OOH may be the cause of accelerated Fe(III) reduction, thereby promoting the activation of H_2O_2 to generate abundant •OH, further leading to the autocatalytic degradation of pollutants.

The steady-state concentration of •OH in Fe(III)/H_2O_2 system was investigated using nitrobenzene (NB) as the probe ($k_{•OH,\ NB} = 3.9 \times 10^9$ $M^{-1}{\cdot}s^{-1}$) [70]. As shown in Fig. S35, as PCM concentration increased from 0.0 to 20.0 mg/L, the rate constants (k) of NB degradation increased from $(2.03 \pm 0.12) \times 10^{-2}$ to $(9.35 \pm 0.24) \times 10^{-2}$ min^{-1}, thereby the corresponding •OH steady-state concentration increased from $(0.87 \pm 0.05) \times 10^{-13}$ to $(4.00 \pm 0.10) \times 10^{-13}$ M (Table S9), suggesting that •OH generation in Fe(III)/H_2O_2 system was significantly enhanced due to the involvement of phenolic moiety.

3.4. Plausible mechanism

The kinetics and spectroscopic measurements in the oxidation of phenolic pollutant (P) by Fe(III)/H_2O_2 allowed us to propose the following self-catalytic mechanism (Eqs. 10–18).

$$Fe(III) + P \rightarrow P\text{-}Fe(III) \quad (10)$$

$$P\text{-}Fe(III) + H_2O_2 \rightarrow P\text{-}Fe(III)\text{-}OOH + H^- \quad (11)$$

$$P\text{-}Fe(III)\text{-}OOH \rightarrow Fe(II) + P + HO_2^{\bullet} \quad (12)$$

$$Fe(II) + H_2O_2 \rightarrow Fe(III) + •OH + OH^- \quad (13)$$

$$P + •OH \rightarrow Q \quad (14)$$

$$Fe(III) + Q + H_2O_2 \rightarrow\rightarrow\rightarrow\rightarrow Fe(II) + Q + HO_2^{\bullet} \quad (15)$$

$$Q + •OH \rightarrow \text{Oxidized products} \quad (16)$$

$$4\ •OH \rightarrow {}^1O_2 + 2\ H_2O \quad (17)$$

$$P + {}^1O_2 \rightarrow \text{Oxidized products} \quad (18)$$

In the initiation stage, the active Fe(III) interacts with phenolic pollutants in the absence of H_2O_2 to form P-Fe(III) complex (Eq. 10) [14]. Once H_2O_2 is added, the pre-generated P-Fe(III) complex can be transformed into P-Fe(III)-OOH (Eq. 11). Subsequently, the high-spin

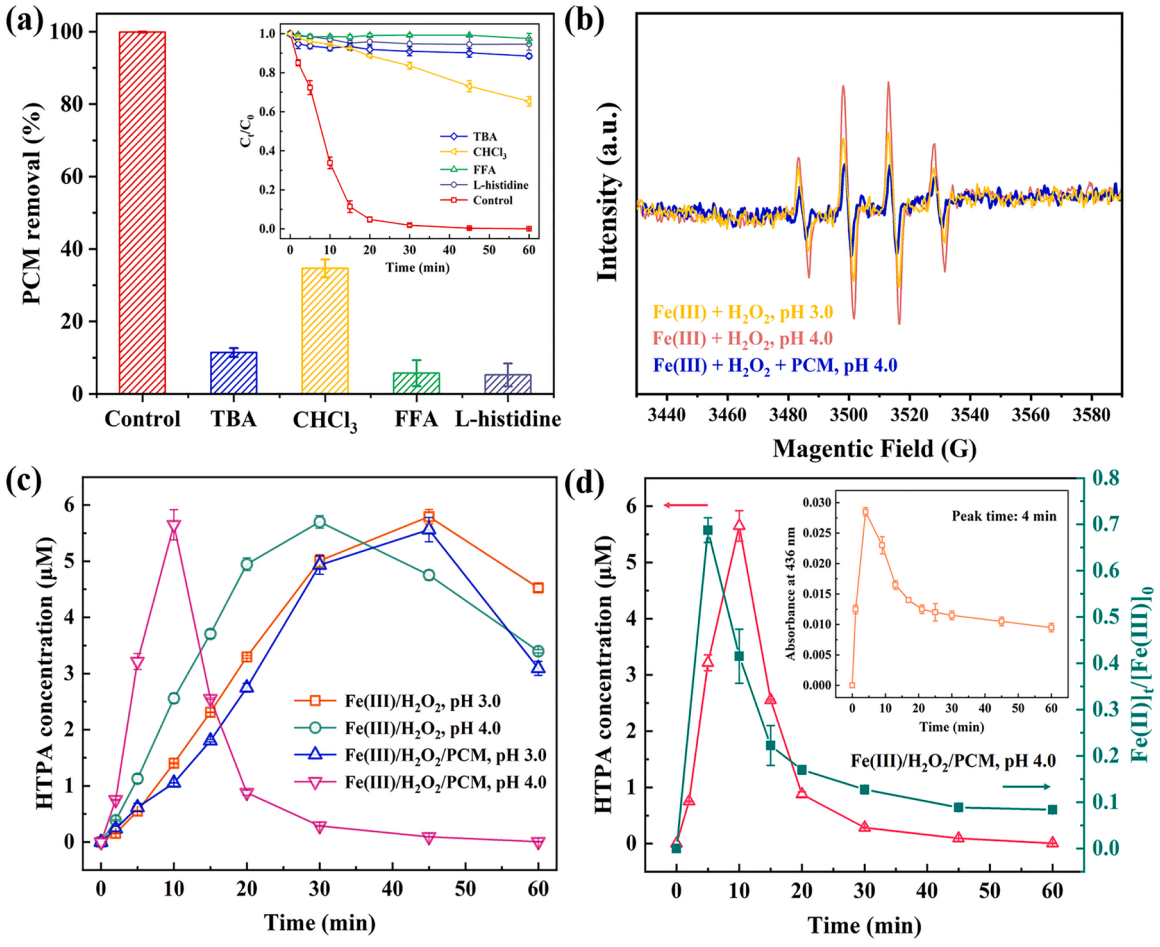

Fig. 4. (a) Effect of different quenchants on PCM degradation in Fe(III)/H_2O_2/PCM system; (b) ESR spectra for detection of DMPO-•OH adducts; (c) Semi-quantitative analysis of •OH in Fe(III)/H_2O_2 systems with TPA as a probe: variations of HTPA; (d) Time profiles of HTPA concentration, $[Fe(II)]_t/[Fe(III)]_0$ and absorbance at 436 nm (inset) in Fe(III)/H_2O_2 system. If no otherwise specified, $[Fe(III)]_0 = 40.0$ μM, $[H_2O_2]_0 = 2.0$ mM, $[PCM]_0 = 10.0$ mg/L, $[quenchant]_0 = 20.0$ mM, $[TPA]_0 = 50$ μM, pH 4.0 and T = 25 °C.

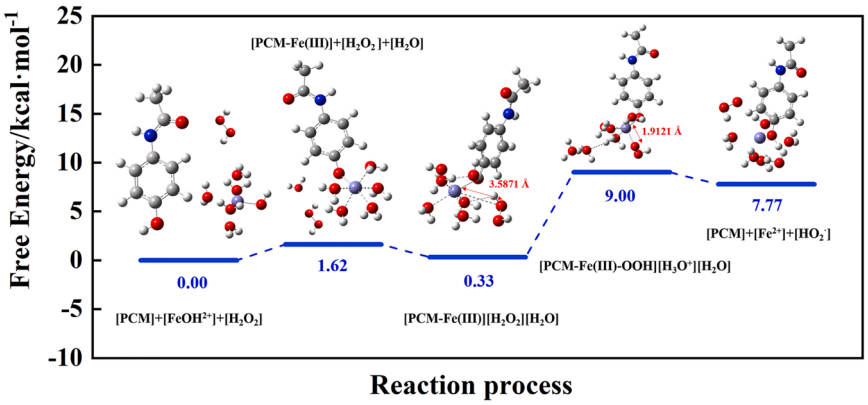

Fig. 5. Relative free energy profile of the initiation of PCM autocatalytic degradation in Fe(III)/H_2O_2 system.

P-Fe(III)-OOH undergoes a rapid homolysis to produce $HO_2^{\bullet}$ due to the weak Fe-O bond [52,71], at the same time, Fe(III) is promptly reduced to Fe(II), which further results in the activation of H_2O_2 to generate •OH (Eqs. 12–13) and triggers the self-catalytic degradation of phenolic pollutant. The enhanced DMPO-$HO_2^{\bullet}$/$O_2^{\bullet-}$ signal in the presence of PCM in ESR spectra (Fig. S36) favors the occurrence of Eq. 12, and the obtained $HO_2^{\bullet}$ is also beneficial to the regeneration of Fe(II) (Eq. 4).

Basically, the oxidation of P by •OH produces quinones (Q, e.g., 1,4-hydroquinone) (Eq. 14), which can also complex with Fe(III) that goes through similar reactions like P-Fe(III) complex with H_2O_2 (i.e., Eqs. 10–12) to produce Fe(II) and finally be completely degraded (Eqs. 15–16). Besides, hydroquinone intermediates accumulated during phenolics degradation (Eq. 14) can serve as the "secondary engine" to further promote the formation of Fe(II) through quinone cycle (Eqs. 6–7), thus improving the pollutant removal performance. Therefore, the generated P-Fe(III)-OOH and quinone intermediates successively facilitated the mutual conversion of Fe(III)/Fe(II) and the activation of H_2O_2, accounting for the self-catalysis in the removal of phenolic moiety containing pollutants.

The effect of pH on the self-catalytic degradation of phenolic pollutants may be understood by considering the variation of the speciation of Fe(III) with pH. Figs. S37 and S38 show the existing form of Fe(III) and PCM-Fe(III) complex at different pH values simulated by MINTEQ software. $FeOH^{2+}$ is the dominant Fe(III) species in the pH range of 2.0–4.0, whereas it is only ~5.0 % at pH 5.0. It is reported that $FeOH^{2+}$ owns higher reactivity, and tends to form complexes with higher redox potential [26,30]. Thus, the open-circuit potential of PCM solution after adding Fe(III) and H_2O_2 at different pH conditions was monitored by chronopotentiometry. As shown in Fig. S39, in any case, the potential of PCM solution increased immediately after the addition of Fe(III) at 600 s, and the potential of solution with an initial pH of 4.0 increased the most. This result indicates that the reactivity of PCM-Fe(III) complex increases sharply at pH 4.0, making it more liable to react with H_2O_2 and trigger the next series of autocatalytic reactions. Interestingly, after the addition of H_2O_2, the potential at pH 4.0 also showed an "S-shaped" curve, which matched well with the autocatalytic process. The transient rise after adding H_2O_2 may herald the formation of PCM-Fe(III)-OOH. Afterwards, the self-catalytic degradation of PCM was initiated, resulting a remarkable descent in potential. Fig. S40 displayed the elevated potential of PCM solution after adding Fe(III) and the final potential of PCM-Fe(III) after complexing for 600 s. A relatively low potential value was observed at pH 5.0, which further explained the poor degradation performance of PCM in Fe(III)/H_2O_2 system at pH 5.0. During the autocatalytic initiation process, pH affects the complexation of phenolic compounds with Fe(III) and H_2O_2, the key step to produce Fe(II) for H_2O_2 activation, thus •OH production is obviously influenced by the pH variation in the range of 3.0–5.0.

The oxidation of PCM at different pH was further understood by carrying out the kinetic measurements at different temperatures. As shown in Fig. S41 the increase of temperature markedly improved the degradation efficiencies at pH 2.4, 3.0 and 4.0, whereas no promotion effect was observed at pH 5.0. The apparent activation energy (E_a), which reflects the basic reaction energy barrier in macroscale [70], was calculated by Arrhenius equation (Text S10 and Fig. S42). The values of E_a of Fe(III)/H_2O_2/PCM system at pH 2.4 and 3.0 were obtained as (120.8 ± 6.2) and (108.5 ± 4.9) kJ•mol^{-1}, respectively. Once the pH was adjusted to 4.0, E_a dramatically dropped to (35.9 ± 2.0) kJ•mol^{-1}. The much lower E_a may be ascribed to the fact that the moderately increased pH reduces the cracking energy barrier of H-O bond in H_2O_2 [41], which is beneficial to the production of PCM-Fe(III)-OOH intermediate to initiate the autocatalytic process. Further evidence showed that the accumulation rate of absorbance at 436 nm at pH 4.0 far exceeded that at pH 2.4 and 3.0 (see Fig. S43).

Finally, DFT calculations were performed to further support the mechanism. The calculated free energy profiles of the autocatalytic initial stage (Eqs. 10–12) were displayed in Fig. 5. It can be seen that the reaction process starts with the complexation of $FeOH(H_2O)_5^{2+}$ and PCM molecule. After that, the iron site of the formed complex attracts H_2O_2, gradually shortening the Fe-O distance from 3.5871 to 1.9121 Å to form Fe(III) hydroperoxide. However, the Fe-O bond in high-spin PCM-Fe(III)-OOH is prone to elongate and break, which is consistent with its fleeting characteristics. During the fracture process, Fe(III) is quickly reduced to Fe(II) through electron transfer. It is worth mentioning that the energy barrier for PCM-Fe(III)-OOH formation (8.67 kcal·mol^{-1}) and Fe(III) reduction (−1.23 kcal·mol^{-1}) is much lower than the reaction barrier at room temperature (21.00 kcal·mol^{-1}), suggesting that these reactions are thermodynamically favorable and can proceed spontaneously with rapid kinetics [72,73]. Through an exothermic process, $Fe(H_2O)_6^{2+}$ and $HO_2^{\bullet}$ are eventually released into the solution to further promote the activation of H_2O_2. Comparatively, the formation of Fe(II) and $HO_2^{\bullet}$ in Fe(III)/H_2O_2 system without PCM requires higher energy (39.65 kcal·mol^{-1}) (Fig. S44). This again supports the role of PCM for the accelerated reduction of Fe(III) in Fe(III)/H_2O_2 system to proceeding the autocatalytic initiation reactions.

4. Conclusion

Phenolic moiety-mediated Fe(III)/H_2O_2 system was found to have the ability to degrade a variety of contaminants under a moderately acid condition, especially the efficient degradation of phenolic contaminants through the formation of Fe(III) hydroperoxide complex with phenolic pollutant itself as the ligands (i.e., P-Fe(III)-OOH complexes) to initiate self-catalytic processes. The gradually generated hydroquinone intermediates from phenolic pollutants degradation further thrust the burst of Fe(II) and •OH, realizing the enhanced degradation performance. Importantly, the refractory pollutants can also be degraded

during the simultaneous oxidation of phenolics. Thus, since phenolic compounds are commonly detected in industrial effluents such as pharmaceutical wastewater, and printing and dyeing wastewater, it is possible to achieve an exceptional efficiency for degradation of co-existing pollutants by constantly feeding phenolic effluents. In addition, the components such as Cl^-, HCO_3^- and humic acid existing in real water hardly affected the performance of PCM removal in Fe(III)/H_2O_2 system (Figs. S45–S46), and the significantly decreased toxicity of PCM after the self-catalytic treatment also indicated that this Fenton-like process could alleviate the potential hazard of pollutants on environment (Fig. S47).

Overall, the study provides a novel strategy to have phenolic pollutant mediated Fenton-like reaction to obtain efficient elimination of refractory organic pollutants in water and wastewater purification. In further scale-up applications, the proportion of phenolic compound, Fe (III) and H_2O_2 requires careful consideration, and irrelevant competing ligand should be excluded in advance.

CRediT authorship contribution statement

Cheng Chen: Conceptualization, Investigation, Methodology, Formal analysis, Writing – original draft. **Yongyi Wang:** Investigation, Visualization. **Yajing Huang:** Validation, Writing – review & editing. **Jian Hua:** Software, Visualization. **Wei Qu**: Validation, Supervision. **Dehua Xia:** Supervision, Funding acquisition. **Chun He:** Resources, Supervision, Funding acquisition, Writing – review & editing. **Virender K. Sharma:** Writing – review & editing, Conceptualization, Methodology. **Dong Shu:** Validation, Supervision.

Declaration of Competing Interest

The authors declare that they have no known competing financial interests or personal relationships that could have appeared to influence the work reported in this paper.

Data availability

Data will be made available on request.

Acknowledgements

The authors wish to thank the National Natural Science Foundation of China (Nos. 21876212, 52070195, 21976214, 41603097, 21673086), Science and Technology Research Programs of Guangdong Province (No. 2019A1515011015), the Science and Technology Program of Guangzhou (No. 201904010353), and Fundamental Research Funds for the Central Universities (Nos. 19lgpy157 and 22lgqb21) for financially supporting this work. Dr. Xia was also supported by Guangdong Basic and Applied Basic Research Foundation (No. 2022B1515020097), Opening Fund of the State Key Laboratory of Environmental Geochemistry (No. SKLEG2022221), and the Start-up Funds for High-Level Talents of Sun Yat-sen University (38000-18821111).

Appendix A. Supporting information

Supplementary data associated with this article can be found in the online version at doi:10.1016/j.apcatb.2022.122062.

References

[1] G. Jungclaus, V. Avila, R. Hites, Organic compounds in an industrial Wastewater: a case study of their environmental impact, Environ. Sci. Technol. 12 (1978) 88–96.
[2] W. Zhong, D. Wang, Z. Wang, Distribution and potential ecological risk of 50 phenolic compounds in three rivers in Tianjin, China, Environ. Pollut. 235 (2018) 121–128.
[3] W. Raza, J. Lee, N. Raza, Y. Luo, K.-H. Kim, J. Yang, Removal of phenolic compounds from industrial waste water based on membrane-based technologies, J. Ind. Eng. Chem. 71 (2019) 1–18.
[4] R. M.K, G. V, UV/solar light induced photocatalytic degradation of phenols and dyes by Fe(PS-BBP)Cl_3, J. Photochem. Photobiol. A Chem. 353 (2018) 477–487.
[5] K. Zhang, Q. Wang, Y. Zhou, J. Gao, C. Li, X. Jiang, A low-cost crosslinked polystyrene derived from environmental wastes for adsorption of phenolic compounds from aqueous solution, J. Mol. Liq. 314 (2020), 113641.
[6] F. Chen, W. Ma, J. He, J. Zhao, Fenton degradation of malachite green catalyzed by aromatic additives, J. Phys. Chem. A 106 (2002) 9485–9490.
[7] J.J. Pignatello, D. Liu, P. Huston, Evidence for an additional oxidant in the photoassisted fenton reaction, Environ. Sci. Technol. 33 (1999) 1832–1839.
[8] M. Yang, Z. Hou, X. Zhang, B. Gao, Y. Li, Y. Shang, Q. Yue, X. Duan, X. Xu, Unveiling the origins of selective oxidation in single-atom catalysis via Co–N_4–C intensified radical and nonradical pathways, Environ. Sci. Technol. 56 (2022) 11635–11645.
[9] W. Gernjak, T. Krutzler, A. Glaser, S. Malato, J. Caceres, R. Bauer, A.R. Fernández-Alba, Photo-Fenton treatment of water containing natural phenolic pollutants, Chemosphere 50 (2003) 71–78.
[10] P. Zhou, W. Ren, G. Nie, X. Li, X. Duan, Y. Zhang, S. Wang, Fast and long-lasting iron(III) reduction by boron toward green and accelerated Fenton chemistry, Angew. Chem. Int. Ed. 59 (2020) 16517–16526.
[11] D. Tang, G. Zhang, F. Chen, J. Ma, Cocatalyst or substrate? Competitive Fenton transformation of cysteine and salicylic acid, Environ. Sci. Water Res. Technol. 5 (2019) 1046–1053.
[12] Q. Yan, J. Zhang, M. Xing, Cocatalytic Fenton reaction for pollutant control, Cell Rep. Phys. Sci. 1 (2020), 100149.
[13] W. Qu, C. Chen, Z. Tang, D. Xia, D. Ma, Y. Huang, Q. Lian, C. He, D. Shu, B. Han, Electron-rich/poor reaction sites enable ultrafast confining Fenton-like processes in facet-engineered BiOI membranes for water purification, Appl. Catal. B Environ. 304 (2022), 120970.
[14] F.J. Rivas, F.J. Beltrán, J.F. Garcia-araya, V. Navarrete, O. Gimeno, Co-oxidation of *p*-hydroxybenzoic acid and atrazine by the Fenton's like system Fe(III)/H_2O_2, J. Hazard. Mater. 91 (2002) 143–157.
[15] F. Herrera, J. Kiwi, A. Lopez, V. Nadtochenko, Photochemical decoloration of Remazol Brilliant Blue and Uniblue A in the presence of Fe^{3+} and H_2O_2, Environ. Sci. Technol. 33 (1999) 3145–3151.
[16] F. Chen, Y. Li, L. Guo, J. Zhang, Strategies comparison of eliminating the passivation of non-aromatic intermediates in degradation of Orange II by Fe^{3+}/H_2O_2, J. Hazard. Mater. 169 (2009) 711–718.
[17] J. Ma, W. Song, C. Chen, W. Ma, J. Zhao, Y. Tang, Fenton degradation of organic compounds promoted by dyes under visible irradiation, Environ. Sci. Technol. 39 (2005) 5810–5815.
[18] J. Bolobajev, M. Trapido, A. Goi, Improvement in iron activation ability of alachlor Fenton-like oxidation by ascorbic acid, Chem. Eng. J. 281 (2015) 566–574.
[19] Y. Qin, F. Song, Z. Ai, P. Zhang, L. Zhang, Protocatechuic acid promoted alachlor degradation in Fe(III)/H_2O_2 Fenton system, Environ. Sci. Technol. 49 (2015) 7948–7956.
[20] T. Pan, Y. Wang, X. Yang, X.-f Huang, R.-l Qiu, Gallic acid accelerated BDE47 degradation in PMS/Fe(III) system: oxidation intermediates autocatalyzed redox cycling of iron, Chem. Eng. J. 384 (2020), 123248.
[21] H. Dong, C. Sans, W. Li, Z. Qiang, Promoted discoloration of methyl orange in H_2O_2/Fe(III) Fenton system: effects of gallic acid on iron cycling, Sep. Purif. Technol. 171 (2016) 144–150.
[22] T. Li, Z. Zhao, Q. Wang, P. Xie, J. Ma, Strongly enhanced Fenton degradation of organic pollutants by cysteine: an aliphatic amino acid accelerator outweighs hydroquinone analogues, Water Res. 105 (2016) 479–486.
[23] J. Liu, C. Dong, Y. Deng, J. Ji, S. Bao, C. Chen, B. Shen, J. Zhang, M. Xing, Molybdenum sulfide Co-catalytic Fenton reaction for rapid and efficient inactivation of Escherichia coli, Water Res. 145 (2018) 312–320.
[24] M. Xing, W. Xu, C. Dong, Y. Bai, J. Zeng, Y. Zhou, J. Zhang, Y. Yin, Metal sulfides as excellent co-catalysts for H_2O_2 decomposition in advanced oxidation processes, Chem 4 (2018) 1359–1372.
[25] L. Zhu, J. Ji, J. Liu, S. Mine, M. Matsuoka, J. Zhang, M. Xing, Designing 3D-MoS_2 sponge as excellent cocatalysts in advanced oxidation processes for pollutant control, Angew. Chem. Int. Ed. 59 (2020) 13968–13976.
[26] J. Ji, R.M. Aleisa, H. Duan, J. Zhang, Y. Yin, M. Xing, Metallic active sites on MoO_2(110) surface to catalyze advanced oxidation processes for efficient pollutant removal, iScience 23 (2020), 100861.
[27] Y. Xiao, J. Ji, L. Zhu, Y. Bao, X. Liu, J. Zhang, M. Xing, Regeneration of zero-valent iron powder by the cocatalytic effect of WS_2 in the environmental applications, Chem. Eng. J. 383 (2020), 123158.
[28] C. Dong, J. Ji, B. Shen, M. Xing, J. Zhang, Enhancement of H_2O_2 decomposition by the co-catalytic effect of WS_2 on the Fenton reaction for the synchronous reduction of Cr(VI) and remediation of phenol, Environ. Sci. Technol. 52 (2018) 11297–11308.
[29] H. Zhou, Z. Xie, Y. Liu, B. Lai, W.-J. Ong, S. Wang, X. Duan, Recent advances in molybdenum disulfide-based advanced oxidation processes, Environ. Funct. Mater. 1 (2022) 1–9.
[30] Q. Yi, J. Ji, B. Shen, C. Dong, J. Liu, J. Zhang, M. Xing, Singlet oxygen triggered by superoxide radicals in a molybdenum cocatalytic fenton reaction with enhanced REDOX activity in the environment, Environ. Sci. Technol. 53 (2019) 9725–9733.
[31] Z. Yang, A. Yu, C. Shan, G. Gao, B. Pan, Enhanced Fe(III)-mediated Fenton oxidation of atrazine in the presence of functionalized multi-walled carbon nanotubes, Water Res. 137 (2018) 37–46.

[32] H. Zhou, J. Peng, J. Li, J. You, L. Lai, R. Liu, Z. Ao, G. Yao, B. Lai, Metal-free black-red phosphorus as an efficient heterogeneous reductant to boost Fe^{3+}/Fe^{2+} cycle for peroxymonosulfate activation, Water Res. 188 (2021), 116529.
[33] R. Chen, J.J. Pignatello, Role of quinone intermediates as electron shuttles in Fenton and photoassisted fenton oxidations of aromatic compounds, Environ. Sci. Technol. 31 (1997) 2399–2406.
[34] J. Feng, S. Li, Y. Sheng, Y. Xiong, S. Lan, S. Tian, L. Kong, C. Fan, Remarkable improvement of cycling Fenton process for catalytic degradation of phenol: tuning of triggering effect, Appl. Catal. A Gen. 542 (2017) 21–27.
[35] H. Tamura, K. Goto, T. Yotsuyanagi, M. Nagayama, Spectrophotometric determination of iron(II) with 1,10-phenanthroline in the presence of large amounts of iron(III), Talanta 21 (1974) 314–318.
[36] R.F.P. Nogueira, M.C. Oliveira, W.C. Paterlini, Simple and fast spectrophotometric determination of H_2O_2 in photo-Fenton reactions using metavanadate, Talanta 66 (2005) 86–91.
[37] J. Ding, H. Nie, S. Wang, Y. Chen, Y. Wan, J. Wang, H. Xiao, S. Yue, J. Ma, P. Xie, Transformation of acetaminophen in solution containing both peroxymonosulfate and chlorine: performance, mechanism, and disinfection by-product formation, Water Res. 189 (2021), 116605.
[38] L. Peng, Y. Shang, B. Gao, X. Xu, Co_3O_4 anchored in N, S heteroatom co-doped porous carbons for degradation of organic contaminant: role of pyridinic N-Co binding and high tolerance of chloride, Appl. Catal. B Environ. 282 (2021), 119484.
[39] C. Chen, T. Ma, Y. Shang, B. Gao, B. Jin, H. Dan, Q. Li, Q. Yue, Y. Li, Y. Wang, X. Xu, In-situ pyrolysis of Enteromorpha as carbocatalyst for catalytic removal of organic contaminants: considering the intrinsic N/Fe in Enteromorpha and non-radical reaction, Appl. Catal. B Environ. 250 (2019) 382–395.
[40] R. Thakura, S. Chakrabortty, P. Pal, Treating complex industrial wastewater in a new membrane-integrated closed loop system for recovery and reuse, Clean. Technol. Environ. Policy 17 (2015) 2299–2310.
[41] S. Lan, Y. Xiong, S. Tian, J. Feng, T. Xie, Enhanced self-catalytic degradation of CuEDTA in the presence of H_2O_2/UV: Evidence and importance of Cu-peroxide as a photo-active intermediate, Appl. Catal. B Environ. 183 (2016) 371–376.
[42] S. Yanan, X. Xing, Q. Yue, B. Gao, Y. Li, Nitrogen-doped carbon nanotubes encapsulating Fe/Zn nanoparticles as a persulfate activator for sulfamethoxazole degradation: role of encapsulated bimetallic nanoparticles and nonradical reaction, Environ. Sci. Nano 7 (2020) 1444–1453.
[43] J. Cho, S. Jeon, S.A. Wilson, L.V. Liu, E.A. Kang, J.J. Braymer, M.H. Lim, B. Hedman, K.O. Hodgson, J.S. Valentine, E.I. Solomon, W. Nam, Structure and reactivity of a mononuclear non-haem iron(III)-peroxo complex, Nature 478 (2011) 502–505.
[44] H. Kim, P.J. Rogler, S.K. Sharma, A.W. Schaefer, E.I. Solomon, K.D. Karlin, Heme-feiii superoxide, peroxide and hydroperoxide thermodynamic relationships: Fe^{III}-$O_2^{\bullet-}$ complex H-atom abstraction reactivity, J. Am. Chem. Soc. 142 (2020) 3104–3116.
[45] V.K. Sharma, P.Á. Szilágyi, Z. Homonnay, E. Kuzmann, A. Vértes, Mössbauer investigation of peroxo species in the iron(III)–EDTA–H_2O_2 system, Eur. J. Inorg. Chem. 2005 (2005) 4393–4400.
[46] G. Roelfes, V. Vrajmasu, K. Chen, R.Y.N. Ho, J.-U. Rohde, C. Zondervan, R.M. la Crois, E.P. Schudde, M. Lutz, A.L. Spek, R. Hage, B.L. Feringa, E. Münck, L. Que, End-on and side-on peroxo derivatives of non-heme iron complexes with pentadentate ligands: models for putative intermediates in biological iron/dioxygen chemistry, Inorg. Chem. 42 (2003) 2639–2653.
[47] F. Grandjean, L. Samain, G.J. Long, Characterization and utilization of Prussian blue and its pigments, Dalton Trans. 45 (2016) 18018–18044.
[48] S. Liang, L. Zhu, J. Hua, W. Duan, P.-T. Yang, S.-L. Wang, C. Wei, C. Liu, C. Feng, Fe^{2+}/HClO reaction produces $Fe^{IV}O^{2+}$: an enhanced advanced oxidation process, Environ. Sci. Technol. 54 (2020) 6406–6414.
[49] U.I. Kramm, L. Ni, S. Wagner, ^{57}Fe Mössbauer spectroscopy characterization of electrocatalysts, Adv. Mater. 31 (2019), 1805623.
[50] Y. Xing, Z. Yao, W. Li, W. Wu, X. Lu, J. Tian, Z. Li, H. Hu, M. Wu, Fe/Fe_3C boosts H_2O_2 utilization for methane conversion overwhelming O_2 generation, Angew. Chem. Int. Ed. 60 (2021) 8889–8895.
[51] S.M. Hölzl, P.J. Altmann, J.W. Kück, F.E. Kühn, Speciation in iron epoxidation catalysis: a perspective on the discovery and role of non-heme iron(III)-hydroperoxo species in iron-catalyzed oxidation reactions, Coord. Chem. Rev. 352 (2017) 517–536.
[52] Z. Yang, C. Shan, B. Pan, J.J. Pignatello, The Fenton reaction in water assisted by Picolinic Acid: accelerated iron cycling and co-generation of a selective Fe-based oxidant, Environ. Sci. Technol. 55 (2021) 8299–8308.
[53] Y. Zong, Y. Shao, Y. Zeng, B. Shao, L. Xu, Z. Zhao, W. Liu, D. Wu, Enhanced oxidation of organic contaminants by iron(II)-activated periodate: the significance of high-valent iron–oxo species, Environ. Sci. Technol. 55 (2021) 7634–7642.
[54] M. Chen, Y. Yu, P. Tan, X. Zhou, X. Chen, Q. Cai, R.J. Zeng, S. Zhou, Selective degradation of estrogens by a robust iron(III) complex bearing a cross-bridged cyclam ligand via iron(V)-oxo species, Chem. Eng. J. 378 (2019), 122223.
[55] Z. Wang, J. Jiang, S. Pang, Y. Zhou, C. Guan, Y. Gao, J. Li, Y. Yang, W. Qiu, C. Jiang, Is sulfate radical really generated from peroxydisulfate activated by iron (ii) for environmental decontamination? Environ. Sci. Technol. 52 (2018) 11276–11284.
[56] L. Peng, X. Duan, Y. Shang, B. Gao, X. Xu, Engineered carbon supported single iron atom sites and iron clusters from Fe-rich Enteromorpha for Fenton-like reactions via nonradical pathways, Appl. Catal. B Environ. 287 (2021), 119963.
[57] L. Pan, W. Shi, T. Sen, L. Wang, J. Zhang, Visible light-driven selective organic degradation by $FeTiO_3$/persulfate system: the formation and effect of high valent Fe(IV), Appl. Catal. B Environ. 280 (2021), 119414.
[58] H.-H. Kim, H. Lee, D. Lee, Y.-J. Ko, H. Woo, J. Lee, C. Lee, A.L.-T. Pham, Activation of hydrogen peroxide by a titanium oxide-supported iron catalyst: evidence for surface Fe(IV) and its selectivity, Environ. Sci. Technol. 54 (2020) 15424–15432.
[59] N. Jiang, H. Xu, L. Wang, J. Jiang, T. Zhang, Nonradical oxidation of pollutants with single-atom-Fe(III)-activated persulfate: Fe(V) being the possible intermediate oxidant, Environ. Sci. Technol. 54 (2020) 14057–14065.
[60] B. Shao, H. Dong, B. Sun, X. Guan, Role of ferrate(IV) and ferrate(V) in activating ferrate(VI) by calcium sulfite for enhanced oxidation of organic contaminants, Environ. Sci. Technol. 53 (2019) 894–902.
[61] D. Xia, H. He, H. Liu, Y. Wang, Q. Zhang, Y. Li, A. Lu, C. He, P.K. Wong, Persulfate-mediated catalytic and photocatalytic bacterial inactivation by magnetic natural ilmenite, Appl. Catal. B Environ. 238 (2018) 70–81.
[62] L. Wang, H. Xu, N. Jiang, Z. Wang, J. Jiang, T. Zhang, Trace cupric species triggered decomposition of peroxymonosulfate and degradation of organic pollutants: Cu(III) being the primary and selective intermediate oxidant, Environ. Sci. Technol. 54 (2020) 4686–4694.
[63] F. Wilkinson, J.G. Brummer, Rate constants for the decay and reactions of the lowest electronically excited singlet state of molecular oxygen in solution, J. Phys. Chem. Ref. Data 10 (1981) 809–999.
[64] F. Sun, T. Chen, H. Liu, X. Zou, P. Zhai, Z. Chu, D. Shu, H. Wang, D. Chen, The pH-dependent degradation of sulfadiazine using natural siderite activating PDS: the role of singlet oxygen, Sci. Total Environ. 784 (2021), 147117.
[65] J. Miao, W. Geng, P.J.J. Alvarez, M. Long, 2D N-doped porous carbon derived from polydopamine-coated graphitic carbon nitride for efficient nonradical activation of peroxymonosulfate, Environ. Sci. Technol. 54 (2020) 8473–8481.
[66] D. Xia, H. Liu, B. Xu, Y. Wang, Y. Liao, Y. Huang, L. Ye, C. He, P.K. Wong, R. Qiu, Single Ag atom engineered 3D-MnO_2 porous hollow microspheres for rapid photothermocatalytic inactivation of E. coli under solar light, Appl. Catal. B Environ. 245 (2019) 177–189.
[67] Z. Kozmér, E. Arany, T. Alapi, E. Takács, L. Wojnárovits, A. Dombi, Determination of the rate constant of hydroperoxyl radical reaction with phenol, Radiat. Phys. Chem. 102 (2014) 135–138.
[68] A.A. Gorman, M.A.J. Rodgers, Singlet molecular-oxygen, Chem. Soc. Rev. 10 (1981) 205–231.
[69] P. Zhou, F. Cheng, G. Nie, Y. Yang, K. Hu, X. Duan, Y. Zhang, S. Wang, Boron carbide boosted Fenton-like oxidation: a novel Fe(III)/Fe(II) circulation, Green Energy Environ. 5 (2020) 414–422.
[70] P. Duan, X. Liu, B. Liu, M. Akram, Y. Li, J. Pan, Q. Yue, B. Gao, X. Xu, Effect of phosphate on peroxymonosulfate activation: accelerating generation of sulfate radical and underlying mechanism, Appl. Catal. B Environ. 298 (2021), 120532.
[71] M.R. Bukowski, H.L. Halfen, T.A. van den Berg, J.A. Halfen, L. Que Jr., Spin-state rationale for the peroxo-stabilizing role of the thiolate ligand in superoxide reductase, Angew. Chem. Int. Ed. 44 (2005) 584–587.
[72] M. Luo, H. Zhou, P. Zhou, L. Lai, W. Liu, Z. Ao, G. Yao, H. Zhang, B. Lai, Insights into the role of in-situ and ex-situ hydrogen peroxide for enhanced ferrate(VI) towards oxidation of organic contaminants, Water Res. 203 (2021), 117548.
[73] D.C. Young, Mesoscale Methods, Computational Chemistry2001, 273–276.